Co-phase penetration of WC$(10\bar{1}0)$/WC$(10\bar{1}0)$ grain boundaries from first principles

Mikael Christensen and Göran Wahnström
Department of Applied Physics, Chalmers University of Technology and Göteborg University, SE-412 96 Göteborg, Sweden
(Received 15 October 2002; revised manuscript received 20 December 2002; published 25 March 2003)

We examine different interface energy relationships at the WC$(10\bar{1}0)$ surface in the WC-Co cemented carbide using density-functional theory. To assess the stability of WC/WC grain boundaries, 90°-twist grain boundaries and a 27°-twist grain boundary are considered. In addition, we investigate the adhesion properties at the Co(001)/WC$(10\bar{1}0)$ interface by analyzing twelve different interfacial structures, including both W and C terminations of the carbide. The results indicate that the adhesion properties of Co on WC$(10\bar{1}0)$ can be explained either by a considerable adjustment of the interfacial Co atoms to their interfacial equilibrium positions, or by an interfacial structure where the WC surface has a mixed composition of C and W atoms. Finally, the WC/WC grain boundary and Co/WC interface energy relationships are discussed in the context of liquid-phase sintering.

DOI: 10.1103/PhysRevB.67.115415 PACS number(s): 68.35.−p

I. INTRODUCTION

The WC-Co based cemented carbides constitute a group of industrially important composite materials with high hardness and toughness.[1] They are used in a wide range of applications including cutting tool inserts, rock drills, and tyre studs. The hardness is provided by the carbide and the toughness by the ductile metal binder phase. The combination of WC and Co is particularly successful and has been subject to numerous studies (see, e.g., Ref. 1).

Much effort has been made to relate mechanical properties with the microstructure of the cemented carbide. The microstructure is to a large degree determined by interfacial energy relationships. The relationships between surface energies, Co/WC interfacial energies, and WC grain boundary energies, not only play an important role in the mechanical strength of the material, but are also crucial in the manufacturing of these materials, where powders of the carbide and metal are sintered together. A necessary condition for an effective sintering is that wetting of the metal on the carbide is complete, so that the metal phase efficiently fills the empty voids present in the material; voids that would otherwise deteriorate the mechanical properties.

Unfortunately, it is very hard to get experimental information on the adhesion properties and the related interfacial energies. The traditional experimental methods, i.e., wetting experiments such as sessile drop experiments or dihedral angle measurements, can only provide a qualitative picture of the interface energy relationships. Thus, there is a strong need for supplementary data.

With recent advances in computer technology and theoretical modeling, it has become possible to perform atomistic calculations from first principles of interfaces in composite materials. In a recent study, the Co(001)/WC(001) interface energetics was calculated from first principles and compared with the Co(001)/TiC(001) case using the cubic β phase of WC.[2] The experimental fact of better wetting of Co on WC than on TiC was reproduced by the simulations and explained in terms of the energetics and electronic structure at the interfaces.

The present study explores the characteristics of the Co(001)/WC$(10\bar{1}0)$ metal-carbide interface using the hexagonal form of WC. The cobalt-carbide interactions at the WC(0001) surface are treated elsewhere.[3] In addition to this, it is also necessary to get a good description of the behavior of WC/WC grain boundaries for an understanding of the interplay between the different phases. As a first step to understand the nature of WC/WC grain boundaries, this study addresses pure grain boundaries without segregated Co. Motivated by experimental observations,[4,5] we perform first-principle calculations of grain boundaries formed by matching prismatic $\{10\bar{1}0\}$ WC facets together. We compare the grain-boundary energies with the interface energy of the Co/WC system and discuss the results in the context of liquid-phase sintering.

II. BASIC DEFINITIONS OF INTERFACE ENERGETICS

Our prime objective in this work is to assess the strength and stability of different contact surfaces in the cemented carbide. First-principles calculations using density-functional theory (DFT) (Refs. 6–8) have proven to give an accurate description of interface energetics for a wide range of interface systems. The dominating contribution to the interface energetics is given by the internal energy, i.e., the total energies obtained from DFT. The other terms are assumed to be relatively small,[9] and are not included in the calculations since they should not affect the conclusions in this study. This approximation is further justified by the fact that the temperature-dependent terms tend to cancel for the differences in free energy between the considered structures.[10] All structures are modeled in a supercell slab geometry with periodic boundary conditions.

One easily accessible measure of the interfacial strength is the ideal work of separation W_{sep}. The work of separation gives an estimate of the reversible work required to separate the interface into two free surfaces. All dissipative and chemical equilibrating processes, such as dislocation motion, surface contamination, and diffusional processes are neglected. Thus, the energy needed in a real cleavage experi-

TABLE I. Equilibrium lattice constant a_0, bulk modulus B, and cohesive energy E_{coh} calculated using the plane-wave (PW) pseudopotential method in comparison with other calculations and experimental (Expt.) data. FP-LMTO is the full potential linear muffin-tin orbital method. LMTO-ASA is the potential linear muffin-tin orbital method using the atomic sphere approximation. Results are presented for hexagonal WC (WC hex.) with $c/a=1$, and $c/a=0.976$; and fcc Co where also values for ferromagnetic (FM) Co are given for comparison.

System	Method	Source	a_0 (Å)	B (GPa)	E_{coh} (eV)
WC hex. $c=a$	PW-GGA	This work	2.8945	379	8.14
WC hex. $c/a=0.976$	PW-GGA	This work	2.9205	380	8.15
	FP-LMTO-LDA	Ref. 26	2.88	329	9.72
	LMTO-ASA-LDA	Ref. 27	2.88	413	8.90
	Expt.	Quoted in Ref. 26	2.91	331	8.34
WC fcc	PW-GGA	This work	4.38	371	7.71
	FP-LMTO-LDA	Ref. 26	4.29	319	9.46
Co fcc FM	PW-GGA	This work	3.54	199	5.51
	PW-GGA	Ref. 28	3.52	211	5.3
	PW-GGA	Ref. 29	3.52	205	
	Expt.	Quoted in Ref. 29	3.54		
Co fcc NM	PW-GGA	This work	3.47	245	5.30
	PW-GGA	Ref. 28	3.45	253	5.2

ment will always exceed W_{sep}. In the supercell slab geometry, the work of separation can be calculated as

$$W_{sep}=(E_{sl1}+E_{sl2}-E_{int})/2A, \tag{1}$$

where E_{int} is the total energy of the interface structure, and $E_{sl1,2}$ are the total energies of the separated slabs. The factor 2 takes into account that there are two (identical) interfaces per supercell. If the slabs do not contain any mirror plane, the periodic images of the interface may be nonequivalent. In this case a vacuum region of 10 Å is introduced in the interface supercell which then will contain two free surfaces and one interface. Equation (1) is still valid for the work of separation, provided that the factor 2 is removed.

The stability of the interfaces can be assessed by the interface energy γ. The interface energy is the energy gain to create one unit area of interface from bulk material. The interface energy for a supercell structure is usually obtained by calculating the difference in total energy of the interface structure E_{int} and the total energies of the slabs in their bulk environment $E^{(b)}_{sl1,2}$,

$$\gamma=(E_{int}-E^{(b)}_{sl1}-E^{(b)}_{sl2})/2A. \tag{2}$$

The work of separation and the interface energy are not independent quantities. Their sum is equal to the sum of the surface energies of the separated slabs, $\sigma_{1,2}$, as stated by the Dupré equation,

$$\gamma=\sigma_1+\sigma_2-W_{sep} \tag{3}$$

The surface energies $\sigma_{1,2}$ are calculated as

$$\sigma_{1,2}=(E_{sl1,2}-E^{(b)}_{sl1,2})/2A. \tag{4}$$

III. COMPUTATIONAL DETAILS

All electron structure and total-energy calculations are performed using density-functional theory as implemented in the Vienna *ab initio* simulation package (VASP).[11–14] The exchange-correlation functional is approximated with the Perdew-Wang 1991 version of the generalized gradient approximation (GGA-PW91).[15] The plane-wave pseudopotential method[16] with Vanderbilt ultrasoft pseudopotentials[17,18] is used. The Kohn-Sham equations are solved using a preconditioned residuum minimization scheme with direct inversion in the iterative subspace (RMM-DIIS).[14] The plane-wave cutoff energy is set to at least 21 Ry (286 eV) in all calculations. The Brillouin zone is sampled using the Monkhorst-Pack scheme.[19] The partial occupancies are set using the tetrahedron method with Blöchl corrections.[20] Atomic structure relaxations are performed with a quasi-Newton algorithm, and the structures are optimized until the total energies are converged to at least 1 meV.

To assess the accuracy of the computational method, we perform bulk calculations of the different phases in the cemented carbide. Equilibrium lattice constants and the bulk moduli are obtained by fitting the total energies at different volumes to the Murnaghan equation of state.[21] The results from the bulk calculations are collected in Table I The cohesive energies are given with respect to the energies of the spin-polarized atoms in the ground state. The results in Table I of the bulk phases show good agreement with experimental data and other first-principles calculations. The bulk systems under consideration are well described by GGA which corrects for the inherent tendency of overbinding using local-density approximation (LDA).

IV. BULK PHASES IN WC-CO

In the present work we concentrate on the two phase region of WC and Co. Outside this region, other phases may be

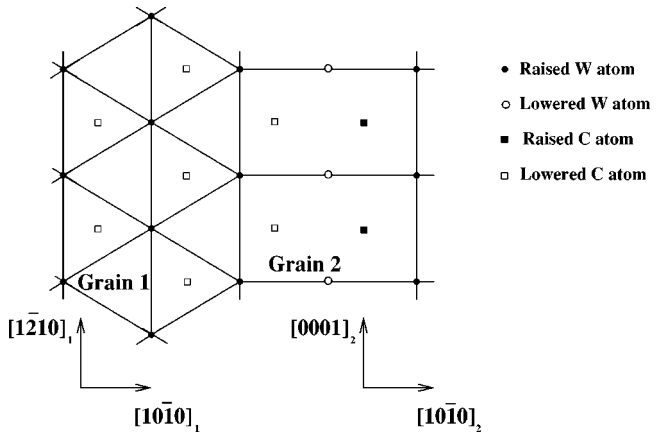

FIG. 1. Schematic picture of the $\Sigma=2$ WC(10$\bar{1}$0)/WC(10$\bar{1}$0) grain boundary.

formed. For example, at high carbon content, carbon will form graphite precipitates, while low carbon content may result in the formation of eta phase precipitates, such as Co_3W_3C. Such precipitates are unwanted in cemented carbides and to a great extent eliminated by careful production methods.

The ground-state crystal structure of the monocarbide WC is simple hexagonal (D_{3h}). It is formed in a narrow range of carbon fraction close to the stoichiometric ratio. This can be compared to group IV-B metal carbides, which have a NaCl structure and are stable over a large range of carbon content. There also exists a NaCl form of WC, the so-called β phase, which can be obtained experimentally at high temperatures (above 2500°C).

In the cemented carbide, the WC grains often take the form of triangular prisms, formed from the basal (0001) plane and three equivalent $\{10\bar{1}0\}$ planes.[22] The c/a ratio is close to 1 (0.976), which gives a possibility for grain boundaries with a very high number of coincidence sites, in particular a $\Sigma=2$ twist grain boundary (Σ is the inverse density of coincidence sites).[4] This is a grain boundary with the orientational relationship $\{10\bar{1}0\}//\{10\bar{1}0\}$, obtained by rotating one grain 90° around the common $\langle 10\bar{1}0\rangle$ axis with respect to the other grain. This special grain boundary has been frequently observed in WC-Co cemented carbides with no evidence of segregated cobalt.[4,5,23–25] If the c/a ratio is approximated by 1, this becomes a pure twist grain boundary with a perfect atomic match of several atomic planes across the contact surface, see Fig. 1. In a real system the slight difference between the a and c parameters will introduce a small mismatch of the interface planes. Experimental observation of the $\Sigma=2$ boundary has shown that this mismatch results in a grain-boundary defect structure consisting of single steps separated by a distance equal to $41a$ or $42c$ (11.9 nm).[23] In our study of WC(10$\bar{1}$0)/WC(10$\bar{1}$0) grain boundaries, we model the coherent regime between steps.

The $\Sigma=2$ grain boundary requires the lattice parameter c in one grain to be equal to the parameter a in the other grain. In modeling this grain boundary, the same values of the parameters have been chosen in both grains. The optimal parameters for WC are found to be $a=c=2.8945$ Å. As can be seen from Table I, the approximation $c=a$ introduces no large errors in the WC bulk properties. This structure of WC is used exclusively in this work.

The electronic structure of WC is well known, and has been investigated in detail using a number of different methods (see, e.g., Refs. 26, 30 and 31). In Ref. 26 it was found that the density of states (DOS) is large at the Fermi level in the NaCl structure of WC, where largely nonbonding d states are occupied. When going to hexagonal WC, the covalent p-d bonds are maintained and the metallic d states are splitted into bonding and antibonding states. The Fermi level is near a minimum in the DOS between bonding and antibonding states. Our calculations show that the DOS for WC with $c=a$ is almost identical to the density of states for the ideal structure, which will be useful in our discussion of the interactions at the interfaces.

The Co binder phase in the WC-Co system can exist in two allotropic forms, hcp or fcc.[32] The high-temperature fcc form of Co is stabilized by residual stresses and the presence of dissolved C and W atoms, and this form is to a large degree retained in the WC-Co cemented carbide. To save computational effort and simplify the analysis, we choose to focus on the paramagnetic fcc phase of Co. This should be a relevant situation in the context of wetting and liquid phase sintering of cemented carbides. The effect of Co ferromagnetism in the Co/TiC system was analyzed in Ref. 33, where it was found that magnetic corrections are not crucial for the conclusions about interface adhesion. It was also found that the magnetic corrections to the interface energetics can be understood within a rigid band approach as for free Co surfaces. To estimate the corrections at the Co/WC interface it then suffices to have the local density of states of the paramagnetic Co interface layer.

V. CLEAN WC SURFACE

There are two options for the location of the WC(10$\bar{1}$0) surface, associated with the two families of (10$\bar{1}$0) planes in WC. These planes consist of either exclusively carbon or tungsten and the distance between consecutive (10$\bar{1}$0) planes in the [10$\bar{1}$0] direction is alternating between 0.836 Å and twice this distance. A cut parallel to the (10$\bar{1}$0) planes may then produce two types of surfaces. In the first case (type-I surface), the distance between the surface atomic layer and the first interlayer is 0.836 Å. In the other case (type-II surface), this distance is twice as large. An important difference between the two types of surfaces is the number of broken bonds. To produce a type-I surface, two neighboring atoms have to be removed per surface atom. The type-II surface is expected to be more reactive, since a cut to produce this surface requires four neighboring atoms to be removed per surface atom. In the present work all surfaces are taken to be ideal, unreconstructed bulk truncations without any adatoms. In the relaxed calculations, the atoms in the three outermost layers are allowed to relax in all directions.

The alternating layers of carbon and tungsten with different spacings in the [10$\bar{1}$0] direction make the (10$\bar{1}$0) planes

TABLE II. Calculated WC($10\bar{1}0$) surface energies $\sigma_W+\sigma_C$. Note that only the sum of surface energies for W and C terminated surfaces is presented. The results for both unrelaxed (Unrel.) and relaxed (Rel.) structures are given.

Surfaces	Unrel. (J/m^2)	Rel. (J/m^2)
W+C I	7.92	7.25
W+C II	14.86	13.86

polar. In periodically repeated supercell structures, such a structure will induce an artificial electrostatic field due to the periodic boundary conditions, which has to be compensated for.

Moreover, supercell calculations of the WC($10\bar{1}0$) surface energy are complicated by the fact that the two surfaces of a stoichiometric slab will always have different atomic terminations. In addition, one of the surfaces of a nonstoichiometric slab will be of type I while the other surface will be of type II, so they are nonidentical. This means that the WC($10\bar{1}0$) surface energy of a particular termination cannot be extracted using a thermodynamical argument by assuming a range of C and W chemical potentials, as has been done for the WC(0001) surface.[34] However, it is enough for our purpose to calculate the sum of the surface energies of W and C terminated surfaces as it appear in Eq. (3). To this end, a stoichiometric slab with eight layers is used. The results are summarized in Table II. As the sum of surface energies indicates, the type-I surfaces are much more stable than the type-II surfaces.

The large difference in surface energies is not reflected in the atomic relaxations. Atomic relaxations are very similar at type-I and type-II surfaces. The largest effect is an inward movement of atoms in the outermost layer of the carbon terminated surfaces of about 0.2 Å. Other relaxations are nearly one order of magnitude smaller.

The WC(0001) surface is also either carbon or tungsten terminated, where the W terminated surface is thermodynamically more stable. The surface energy of the W terminated WC(0001) surface has previously been calculated to about 3.5 J/m^2.[34] Although the only relevant WC($10\bar{1}0$) energies are the sum of tungsten and carbon terminated surfaces $\sigma_W+\sigma_C$, we can get a rough estimate of the relative contributions to this sum by using the same ratio between σ_W and σ_C as calculated in Ref. 34. Using this relation, the relaxed surface energies of the type-I surfaces are found to be $\sigma_C=4.6\pm0.1$ J/m^2 and $\sigma_W=2.7\pm0.1$ J/m^2. The calculated values for the type-II surfaces are $\sigma_C=8.7\pm0.1$ J/m^2 and $\sigma_W=5.2\pm0.1$ J/m^2.

These values are larger than the surface energy of the WC(001) surface of the high-temperature cubic β phase of WC, which has a mixed termination of carbon and tungsten atoms at the surface. Our calculated value of the (unrelaxed) WC(001) surface energy is 1.6 J/m^2. It is interesting to notice that this is close to an experimental value of the WC surface energy of 1.7 J/m^2.[35,36] This could imply that the most stable WC surface is not purely metal terminated. However, the use of GGA generally gives a somewhat low surface energy.[37,38] Using the linear muffin-tin orbitals interface Green's function method with LDA, the WC(001) surface energy was found to be 2.64 J/m^2,[39] which is comparable to our estimate of the W terminated WC($10\bar{1}0$) type-I surface energy.

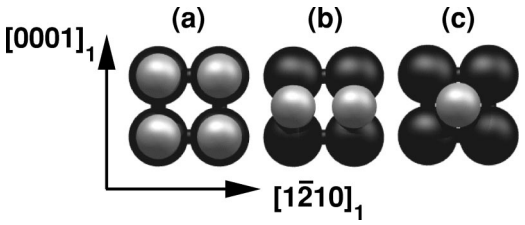

FIG. 2. The three different interfacial atomic configurations studied. The picture shows the relative positions of the atoms closest to the interface in each grain. Dark and light colors correspond to different grains.

There are also experimental studies that indicate that these surfaces are not purely metal terminated, but in fact consist of a mixture of carbon and metal atoms. In a high-resolution core-level-photoemission investigation of the WC(0001) surface, surface shifts were observed both in the carbon and tungsten levels. The result was interpreted as the existence of both carbon and tungsten areas on the surface.[40] Furthermore, a low-energy electron-diffraction structure analysis of WC(0001) indicated that this surface consists of tungsten layer covered by carbon randomly distributed on the hcp sites with a coverage of 30% that of a full carbon layer.[41] Work addressing these questions is in progress.

VI. WC($10\bar{1}0$)/WC($10\bar{1}0$) TWIST GRAIN BOUNDARIES

A. 90°-twist grain boundary

In the present work, we consider grain boundaries formed by matching ($10\bar{1}0$) surfaces of the same type (I or II). Each surface can be either tungsten or carbon terminated. The atomic structure of the interface is determined by four degrees of freedom, the location of the interface plane plus a rigid body displacement **t** of one grain relative to the other. Since we have periodicity in the interface plane, the displacement **t** can be decomposed into a translation **T** parallel to the interface and a component **d** (interface expansion) normal to the interface. If **R** denotes the affine transformation matrix for the 90° rotation around the $\langle 10\bar{1}0\rangle$ axis, and $\mathbf{G}_1$ is a matrix containing the coordinates of the atoms in grain 1, we can write the atomic coordinates $\mathbf{G}_2$ in grain two as

$$\mathbf{G}_2=\mathbf{R}\cdot\mathbf{G}_1+\mathbf{t}. \tag{5}$$

In particular, we will consider three different translation states **T**. Figure 2 shows the relative positions of the atoms in the layers closest to the interface for all translation states. The notation for an interface is of the form *A*-*B*-type-state, where *A* and *B* are the atomic species in the interface layer of grain 1 and 2, respectively, type can be either I or II in accordance with the definition above, and state refers to the three translation states in Fig. 2. For the type-I grain boundary, state *a* corresponds to $\mathbf{T}=(a/2)[0001]_1$, state *b* to **T**

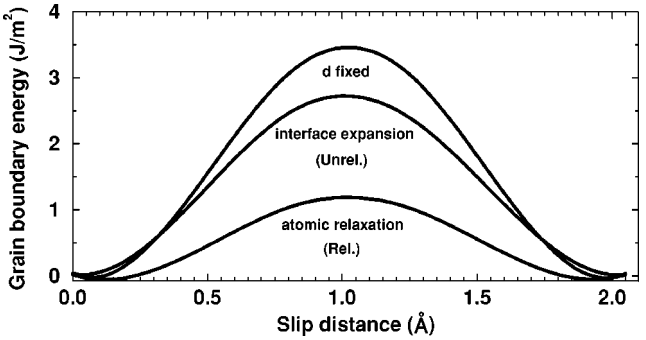

FIG. 3. Cross section of the γ surface of the twist 90° WC($10\bar{1}0$)/WC($10\bar{1}0$) type I grain boundary along the $[1\bar{2}13]$ direction. The upper curve shows the interface energy variation for rigid translations with a fixed intergrain distance d. The middle curve shows the effect of allowing for interface expansion. Full atomic relaxations are included in the bottom curve. No translation corresponds to the $\Sigma=2$ boundary.

$=0$, and state c to $\mathbf{T}=(a/6)[1\bar{2}10]_1$. For the type-II grain boundary, state a corresponds to $\mathbf{T}=(a/6)[1\bar{2}13]_1$, state b to $\mathbf{T}=(a/6)[1\bar{2}10]_1$, and state c to $\mathbf{T}=0$.

For all of these translation states, we calculate the work of separation and interface energy. Both relaxed and unrelaxed values are calculated for all systems. In the relaxed calculations, all atoms in the three outermost layers on each side of each slab are allowed to relaxed in all directions. The supercell size and the atomic positions in the middle layers are kept the same as in the unrelaxed system. As has been shown in earlier studies, the nature of interfaces with more complex structures can adequately be described as superpositions of these more simple coherent interfaces.[2,28]

For the grain-boundary structures, eight atomic layers in each grain [$(10\bar{1}0)$ planes] are used in the calculations. A convergence test with respect to the number of layers is performed, which shows that the energy is converged to within a few mJ/m^2 for a $8+8$ layer supercell.

The relation $\gamma(\mathbf{T})$ describes the γ surface which is a periodic function with the periodicity of the cell of nonidentical displacements (CNID).[42] The CNID consists of all translation vectors parallel to the interface that are not equivalent by the addition of a bicrystal translation vector. However, the two interfaces within the supercell are nonidentical for a general translation state $\mathbf{T}$ due to the WC geometry. Thus, the interface energy given by Eq. (2) is an average value of the two distinct interfaces. Equivalent interfaces are obtained only for some special special cases of translation states. As an example, equivalent interfaces are obtained by a relative displacement of the carbide grains in the $\Sigma 2$ boundary along the $[1\bar{2}13]_1$ direction.

A cross section of the γ surface of the W-C-I grain boundary, obtained by a cubic interpolation of calculated energy values along the the $[1\bar{2}13]_1$ direction is shown in Fig. 3. The $\Sigma=2$ twist boundary is the $\{10\bar{1}0\}//\{10\bar{1}0\}$ interface with the maximum size of the CNID cell. For other twist angles, the density of coincident sites in the boundary is lower and we expect from the restricted form of the maximum planar coincidence site density criterion that the $\Sigma=2$ boundary is a singular boundary.[42] Energy minima of the γ surface are obtained at $\mathbf{T}=0$ and at $\mathbf{T}=(a/6)[1\bar{2}13]_1$, implying that these interfaces are translational singular.

Figure 3 also demonstrates the effect of different types of relaxation. Without any relaxation, the two grains are shifted relative to each other while keeping an interface distance equal to the distance between the atomic planes in bulk. Since the grain-boundary energy to a large degree is determined by the relative positions of the C and W atoms closest to the interface, such a translation can result in large interfacial energies due to repulsion from the large atomic overlap of neighboring atoms across the interface. Allowing for an interface expansion will significantly reduce this interaction energy. The interface expansion may lead to a compressive stress in surrounding grains in the cemented carbide. A rough estimate using the elastic modulus of WC (Ref. 43) indicates that the elastic energy cost for the interface expansion can easily be accommodated by the surrounding grains, at least if they are larger than about 1 nm.

Since the two interfaces within the supercell are nonidentical in the general case, it is not very practical to calculate the interface energy using Eq. (2). A more convenient way is to express the interface energy in terms of the surface energies and the work of separation through the Dupré equation [Eqs. (1), (3), and (4)]. The work of separation for all grain boundaries, together with the optimized interlayer distances d between the grains, is given in Table III. The higher values of the work of separation at type-II boundaries is clearly an effect of a much larger surface energy of the type-II surfaces. The energy differences in W_{sep} between the interfaces gives the relative values of the interface energy γ. For the W-C interfaces, it is possible to calculate the interface energy. The result is given in Table IV. The γ surfaces have local maxima for W-C-I-a, W-C-I-c, W-C-II-a, and W-C-II-b. Minima are obtained at W-C-I-b and W-C-II-c, which corresponds to the relative positions of the atoms in bulk.

The effect of atomic relaxations on the grain boundary energy shown in Fig. 3 is relatively large compared to the effect at the W-C-I-a and W-C-I-c interfaces (Table IV). The large relaxation is due to the fact that the interfacial atoms adjust their positions to the situation given by the singular translation state W-C-I-b. For the high-symmetry W-C-I-a and W-C-I-c interfaces, no in-plane movement of the interfacial atoms occurs during atomic relaxation.

The $\{10\bar{1}0\}$ plane has also been experimentally verified to be the slip plane in WC.[32] Observations have shown that the slip occurs by the motion of $(a/6)\langle 11\bar{2}3\rangle$ partial dislocations. Atomic relaxations significantly lower the energy barrier for an advancement of the interface in the $[1\bar{2}13]_1$ direction. The critical shear stress should be lowest in this direction.

An average value $\bar{\gamma}$ of the WC($10\bar{1}0$)/WC($10\bar{1}0$) grain boundary energy can be obtained by an integration of the γ surface over an interface unit cell,

$$\bar{\gamma}=\int\int_{\text{unit cell}}\gamma(x,y)\,dx\,dy. \tag{6}$$

TABLE III. Work of separation W_{sep} at the WC($10\bar{1}0$)/WC($10\bar{1}0$) grain boundary for all the considered interfacial structures. d is the optimized intergrain distance. Values for both unrelaxed (Unrel.) and relaxed (Rel.) structures are presented.

Interface	Unrel. (J/m^2)	Rel. (J/m^2)	d (Å)
W-C-I-*a*	4.92	4.43	2.02
W-C-I-*b*	7.89	7.22	1.69
W-C-I-*c*	3.24	2.58	1.96
W-C-II-*a*	7.45	6.57	1.95
W-C-II-*b*	10.65	9.92	1.34
W-C-II-*c*	14.83	13.84	0.85
C-C-I-*a*	5.53	4.29	1.46
C-C-I-*b*	0.64	−0.11	1.40
C-C-I-*c*	3.77	2.85	1.40
C-C-II-*a*	13.45	11.73	1.28
C-C-II-*b*	12.09	10.40	0.65
C-C-II-*c*	10.59	8.79	0.07
W-W-I-*a*	5.03	4.99	2.54
W-W-I-*b*	4.88	4.79	2.51
W-W-I-*c*	6.79	6.71	2.18
W-W-II-*a*	3.79	3.62	2.64
W-W-II-*b*	5.29	5.17	2.30
W-W-II-*c*	8.01	7.90	1.97

By a discretization of this integral, and using as sampling points the three translation states a–c (Fig. 2), which are assigned the same weight, the mean value $\bar{\gamma}$ is given by

$$\bar{\gamma} = \frac{1}{4}\{\gamma_a + 2\gamma_b + \gamma_c\}, \tag{7}$$

where γ_a, γ_b, and γ_c are the interface energies of each corresponding translation state. In the same way, a mean value $\bar{W}_{sep}$ of the work of separation can be defined. For the W-C-I boundary the mean values for relaxed structures are,

TABLE IV. Grain boundary energy γ for different WC($10\bar{1}0$)/WC($10\bar{1}0$) grain boundaries. The results for both unrelaxed (Unrel.) and relaxed (Rel.) structures are presented.

Interface	Unrel. (J/m^2)	Rel. (J/m^2)
W-C-I-*a*	3.00	2.82
W-C-I-*b*	0.03	0.02
W-C-I-*c*	4.68	4.67
W-C-II-*a*	7.41	7.29
W-C-II-*b*	4.21	3.94
W-C-II-*c*	0.03	0.02

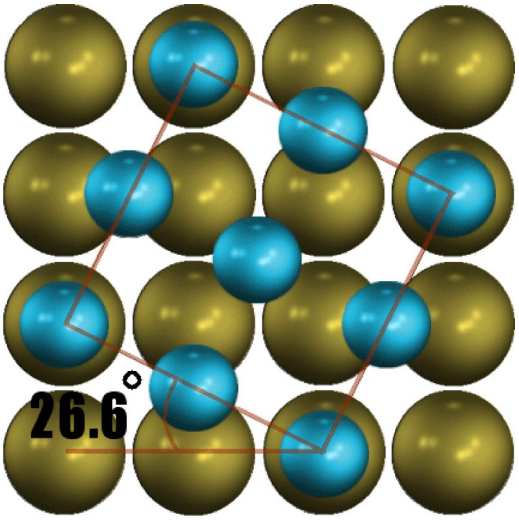

FIG. 4. The relative atomic position of carbon (small) and tungsten (large) atoms at the interface layers at the twist 26.57° WC/WC grain boundary.

$\bar{\gamma} = 1.9$ J/m^2 and $\bar{W}_{sep} = 5.4$ J/m^2. For unrelaxed structures the average values are $\bar{\gamma} = 1.9$ J/m^2 and $\bar{W}_{sep} = 6.0$ J/m^2.

B. 27°-twist grain boundary

In our approach to examine the nature of interfaces, a small number of high-symmetry configurations are considered. If the interfacial energetics is dominated by local interactions, generic boundaries could be described as a mixture of these local configurations. To test this assumption and the representativeness of the model systems, we also consider another type of $\{10\bar{1}0\}//\{10\bar{1}0\}$ type-I grain boundary with a larger misfit.

This boundary is obtained by rotating one grain 26.57° around the $\langle 10\bar{1}0\rangle$ axis, followed by an in-plane stretching of the lattice in one grain by 11.8%. The relaxation of the interplanar distances as an effect of the in-plane stretching is taken into account while the other grain is kept in its bulk state. In the resulting interface unit cell, the ratio of interfacial atoms in grains one and two is 4:5, see Fig. 4. The particular translation state in Fig. 4 can be viewed as consisting of one local configuration *a*, two *b*, and one *c*, from Fig. 2.

The γ surface of this grain boundary is expected to be flatter than for the 90°-twist grain boundary since the CNID is smaller for this more complex interface. An interface with a small CNID has an energy that is insensitive to rigid body translations, and in the ground state it will not support localized dislocations with Burgers vector parallel to the interface. The (unrelaxed) work of separation of the translation state depicted in Fig. 4 is 5.24 J/m^2. This is close to the average value of the work of separation for the 90°-twist boundary, $\bar{W}_{sep}$. Thus, we can conclude that a generic WC($10\bar{1}0$)/WC($10\bar{1}0$) boundary can be described reasonably well within a model based on the considered highly symmetric local configurations. Assuming that the surface

TABLE V. Unrelaxed (Unrel.) and relaxed (Rel.) values of the Co(001) surface energy σ_{Co} for paramagnetic (PM) cobalt.

Surface	Method	Source	Unrel. (J/m^2)	Rel. (J/m^2)
Str. Co PM	PW-GGA	This work	2.80	2.74
Unstr. Co PM	PW-GGA	This work	2.96	2.81
Unstr. Co PM	PW-GGA	Ref. 28	3.04	2.97
Unstr. Co PM	LMTO-ASA-LDA	Ref. 46	3.40	

energy of unstrained WC does not change when a strain is applied, the interface energy can be calculated from the Dupré equation (3) to be 2.69 J/m^2. An interfacial energy of this size is probably typical for grain boundaries approaching the incommensurate limit (CNID goes to zero).

VII. CO/WC INTERFACES

To our knowledge, the details of the Co/WC interface atomic structure are unknown. We analyze the Co(001)/WC(10$\bar{1}$0) interface by considering coherent structures. These are obtained by keeping the carbide in its bulk phase and stretching the softer metal matrix in the interface plane until there is no lattice mismatch across the interface. This results in interface structures with one interface carbide atom per interface Co atom. We also take into account that the in-plane stretch of Co induces a relaxation of the Co interlayer distances. The unstretched fcc lattice can be described as body-centered tetragonal with $c/a=\sqrt{2}$. The strain of the Co lattice required to create completely coherent Co/WC interfaces change the c/a ratio to 0.86. As noted in Ref. 44, a transformation path from fcc to hcp structure consists of a compression of the body-centered-tetragonal (bct) cell until $c/a=\sqrt{2/3}$ together with a shear of the bct (110) planes. The present deformation can then be viewed as a step in this transformation. Linearized-augmented-plane-wave (LAPW) calculations of volume-conserving distortions where the c/a ratio is varied have shown that the strain energy has a shallow local minimum around $c/a=0.9$.[45] The cobalt phase in the present work has a strain energy of 0.35 J/m^2 per Co layer. In spite of the noticeable distortion of Co, the surface energy values differ relatively little from those of the unstrained Co. The Co surface energy is presented in Table V.

The Co/WC supercell consists of eight layers of WC and seven layers of Co plus 10 Å of vacuum. Just as for the WC/WC grain boundaries, we consider the three different translation states depicted in Fig. 2 also for the Co/WC interface. Similarly to the WC surface energy, the interface energy of a specific translation state cannot be determined because of the WC symmetry. Since each supercell contains one interface, a cobalt surface and either a carbon or a tungsten terminated WC surface, we get

$$\gamma_{Co/WC}+\sigma_{Co}+\sigma_{W,C}=(E_{Co/WC}-E_{WC}^{(b)}-E_{Co}^{(b)})/A. \quad (8)$$

By adding together two equations of this form, we get a sum of two Co/WC interface energies which can enter Eq. (10) below. $\gamma_{Co/WC}$ can refer to any of the three translation states. There will also be an additional term given by the sum of WC surface energies. If the two surfaces have different terminations, this sum of surface energies is given in Table II. However, since this additional term also appears in the expression for the grain-boundary energy given by the Dupré equation (3), it will vanish when comparing the Co/WC interface energy with the WC/WC grain-boundary energy. This means that the criterion for Co grain boundary penetration given by Eq. (10) is always computationable.

It is interesting to compare the adhesion properties at the Co(001)/WC(10$\bar{1}$0) interface with the properties at a Co/WC interface where the carbide interface layer does not contain a single atomic species. For this purpose we calculate the Co{001}/WC{100} interface energy, where the cubic β phase of WC is used. The results are in close agreement with the calculations in Ref. 2 using the same computational method, but with a different pseudopotential. The more careful study in Ref. 2 shows that the Co{001}/WC{100} interface energy is about 0.5 J/m^2. This value is very close to experimental results from dihedral angle measurements.[47,48] The work of separation at the Co{001}/WC{100} interface was calculated to be about 3.7 J/m^2. This is close to the wetting experimental value of 3.82 J/m^2.[49] The work of separation at the Co(001)/WC(10$\bar{1}$0) interface is given in Table VI. These values are generally higher than for the Co{001}/WC{100} interface, and thus higher than the experi-

TABLE VI. Work of separation W_{sep} at the Co(001)/WC(10$\bar{1}$0) interface. d is the optimized intergrain distance.

Interface	Unrel. (J/m^2)	Rel. (J/m^2)	d (Å)
C-Co-I-*a*	4.50	4.22	1.81
C-Co-I-*b*	5.50	4.91	1.39
C-Co-I-*c*	2.82	2.20	1.67
W-Co-I-*a*	4.06	4.06	2.23
W-Co-I-*b*	4.59	4.52	2.08
W-Co-I-*c*	5.94	5.87	1.71
C-Co-II-*a*	6.44	5.66	1.70
C-Co-II-*b*	8.97	8.16	1.04
C-Co-II-*c*	11.05	10.30	0.60
W-Co-II-*a*	3.79	3.72	2.26
W-Co-II-*b*	4.73	4.63	1.95
W-Co-II-*c*	7.30	7.23	1.55

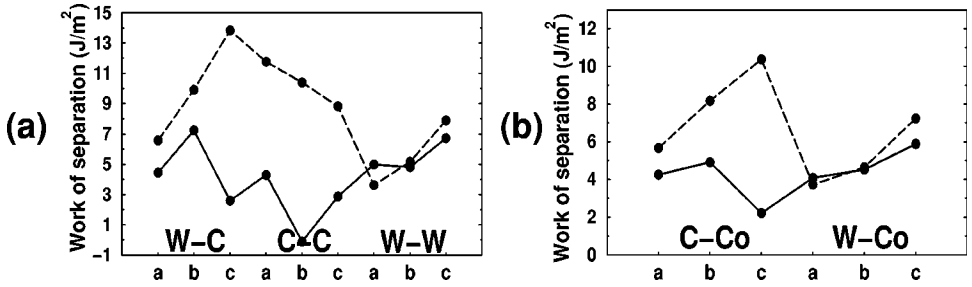

FIG. 5. Work of separation for different interface structures at the WC($10\bar{1}0$)/WC($10\bar{1}0$) (a) and Co(001)/WC($10\bar{1}0$) (b) interfaces. Solid lines correspond to type I and dashed lines to type II interfaces. In (a) the interface structures are W-C-(I,II)-(*a*-*c*), C-C-(I,II)-(*a*-*c*), and W-W-(I,II)-(*a*-*c*). In (b) the structures are C-Co-(I,II)-(*a*-*c*) followed by W-Co-(I,II)-(*a*-*c*).

mental value. These differences are all arguments supporting the assumption indicated in Sec. V, that the clean WC surface is not terminated by a single atomic species. Instead, this indicates that a WC surface with a mixed composition of W and C atoms can explain the adhesion properties of Co on WC.

VIII. DISCUSSION

A. Co-phase penetration of WC grain boundaries

The surface energy relationships in the WC-Co cemented carbide, e.g., the relation between the Co/WC interface energy and the WC/WC grain-boundary energy, are of utmost importance is determining the microstructure of the WC-Co cemented carbide. Properties such as liquid-solid wettability, dihedral angles between grains, and carbide grain growth/size are directly affected by such relations. This also addresses the question whether there is any metal phase between the carbide grains. The ability to form a continuous carbide skeleton greatly improves the mechanical properties of the cemented carbides since plastic deformation of the material requires the whole skeleton to deform.

Comparing the WC/WC grain boundary and Co/WC interface strengths in Figs. 5(a) and 5(b), it can be seen that they are of the same magnitude. No exclusive conclusions can be made about which structure is likely to first break up under an external load. It can be concluded that both WC/WC and Co/WC interfaces are strong and contribute to the advantageous mechanical properties of the WC-Co cemented carbide. The strength of any WC($10\bar{1}0$)/WC($10\bar{1}0$) grain boundary and Co(001)/WC($10\bar{1}0$) interface should be within the limits given by the highest and lowest values of the considered translation states.

The interactions at interfaces involving either a Co or W terminated surface are very similar. Going through the translation states in Fig. 5, the work of separation shows the same trend for both W and Co terminated surfaces. The trend in Co/WC interface energy is also similar between the type-I and type-II interfaces, although there is a much larger variation of the interface energy at type-II interfaces. For all Co/WC interfaces except C-Co-I, it is most energetically favorable to place Co in translation state *c*. The interfacial Co atoms can in this translation state get very close to the WC surface. For the C-Co-I-*c* structure, the W atoms underneath the interface layer are right below the Co atoms, restricting the possibilities for the interfacial atoms to interact effectively. While the smallest type-II interface energy is obtained for the C-Co-II-*c* structure, the corresponding translation state gives the largest interface energy for the type-I interfaces. For C-Co-I it is most favorable to place Co in state *b*, which corresponds to the place the metal atom would have in WC bulk.

To clarify the interactions at the C-Co-I-*c* and C-Co-II-*c* interfaces, we analyze them in terms of their electronic structures. Figure 6 shows ($1\bar{2}13$) cuts of the valence electron density. In the case of C-Co-II-*c* [Fig. 6(b)], there is a large charge accumulation between the interfacial carbon and cobalt atoms, indicative of strong covalent bonds. This includes the Co atoms in the first sublayer, which are positioned directly over the carbon atoms. At the C-Co-I-*c* interface [Fig. 6(a)], the presence of the interface hardly induces any charge at all.

The difference in interfacial interactions is evident in the electronic local density of states (LDOS), given in Fig. 7. The LDOS is projected onto atomic orbitals of the interface atoms. At C-Co-II-*c*, the states of the interfacial atoms are shifted down in energy compared to the bulk states. At C-Co-I-*c*, they are instead shifted upward in energy with approximately the same amount. This is most clearly seen in the region below -10 eV for the C *s* and W *d* states. For the

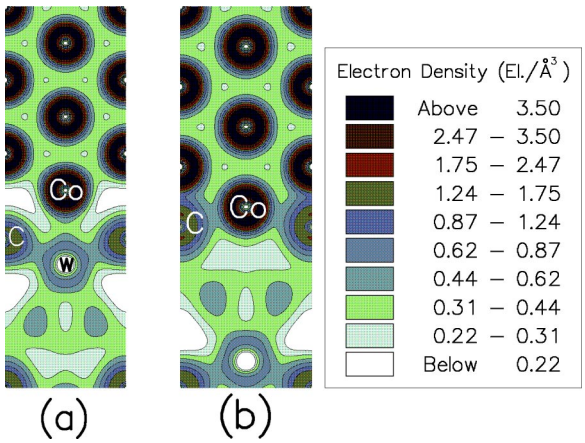

FIG. 6. ($1\bar{2}13$) cuts of the valence electron density for the C-Co-I-*c* (a) and C-Co-II-*c* interfaces. The consecutive contours differ by a factor of $\sqrt{2}$.

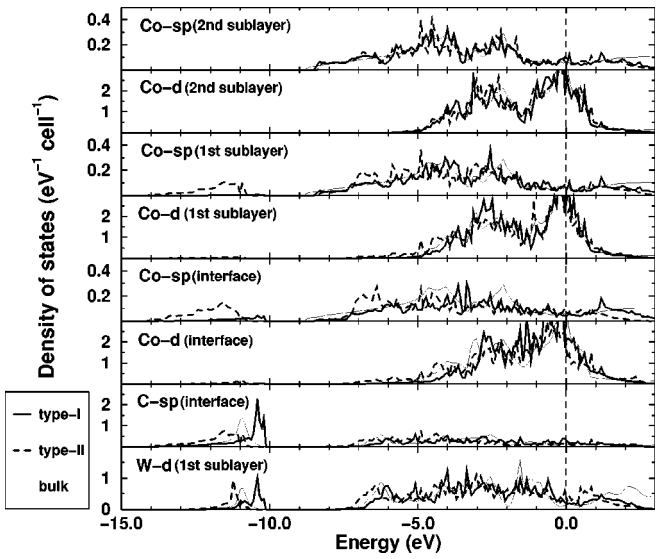

FIG. 7. Layer projected DOS at the C-Co-I-*c* and C-Co-II-*c* interfaces compared to bulk DOS. The DOS for two layers in the carbide and three layers of Co are shown.

Co phase, the presence of the interface affects only states in the two cobalt layers closest to the interface. In the second Co sublayer, the LDOS is very close to the situation in bulk. Interface induced changes in the Co LDOS appear practically only at the C-Co-II-*c* interface, for which the characteristic features are very similar in the interface and first sublayer. At the C-Co-II-*c* interface there is a noticeable hybridization between Co *d* orbitals and C *p* orbitals which gives a broadening at the bottom of Co-*d* band of about 2 eV in the energy region -7 to -5 eV. This shows that the nature of the interfacial Co-C bonds is of the same character as the Co-C bonds at the Co/WC(001)[2] and Co/Ti(C,N)(001) (Ref. 28) interfaces. The C *p* states also modify Co states with more *sp* character, which shows as Co-*sp* peaks at -7 to -6 eV. Note that a different scale is used in Fig. 7 for the Co *sp* states. There are also interface induced Co states in the energy region of the C *s* states around -14 to -9 eV. The similar shapes of the Co *sp* and C *s* states shows that also hybridization involving C *s* orbitals is involved in the interface bonding. None of these features are found at the C-Co-I-*c* interface. This points out the importance of the atomic coordinations and the local interactions at the interface.

Having examined the adhesion properties at the Co/WC interface, it is appropriate to elaborate on their significance in the cemented carbide and the relations to the WC/WC grain-boundary energies. The dihedral angle between carbide grains dispersed in a Co phase is determined by the ratio of $\gamma_{\mathrm{WC/WC}}$ and $\gamma_{\mathrm{Co/WC}}$. At equilibrium, assuming isotropic interface energies, the dihedral angle ϕ is related to the interfacial energies as

$$\gamma_{\mathrm{WC/WC}} = 2\,\gamma_{\mathrm{Co/WC}} \cos\frac{\phi}{2}. \tag{9}$$

This means that when

$$\gamma_{\mathrm{WC/WC}} - 2\,\gamma_{\mathrm{Co/WC}} > 0, \tag{10}$$

there is no value of ϕ which satisfies Eq. (9) and the metal phase will effectively penetrate the WC/WC grain boundaries.

At a semicoherent Co/WC interface, it is reasonable to assume that the softer binder phase more easily adjusts to an interface misfit than the carbide phase. Accordingly, an average value of the interfacial energetics given by Eq. (7) should be a better approximation of a more realistic situation at the WC/WC grain boundaries than at the Co/WC interfaces. It can still be useful to consider this average, as it should give an upper bound on the Co/WC interface energy. Using this approximation, the condition for Co penetration given by Eq. (10) is plotted in Fig. 8(a). Most of the points in the graph are close to the situation where the grain-boundary interface energy is equal to twice the Co/WC interface energy. In this limit, the Co penetration of grain boundaries is therefore inconclusive.

In the other limit, it is assumed that the Co will attach to the WC surfaces so as to minimize the interface energy, i.e., the relative positions of the interface atoms are given by these translation states. The interface misfit will always give a correction to the energy due to, e.g., strain and misfit dislocations,[50] but neglecting these energy contributions gives a lower bound on the Co/WC interface energy. The condition for Co penetration in this idealized case is shown in Fig. 8(b). It can be seen that in general, it is energetically

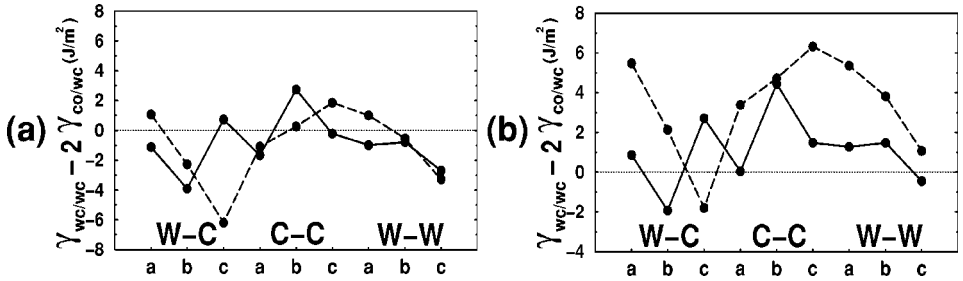

FIG. 8. Comparison of the WC(10$\bar{1}$0)/WC(10$\bar{1}$0) and Co(001)/WC(10$\bar{1}$0) interface energies for type I (solid line) and type II (dashed line) boundaries. In (a), an average value of the Co/WC interface energy for different translation states is used. In (b), the energetically most favorable translation state is used for all interface structures. Along the horizontal axis, the interface structures are W-C-(I,II)-(*a*-*c*), C-C-(I,II)-(*a*-*c*), and W-W-(I,II)-(*a*-*c*). Negative values indicate situations where it is not energetically favorable to have a cobalt phase in the grain boundary.

favorable to have a cobalt phase in WC$(10\bar{1}0)$/WC$(10\bar{1}0)$ grain boundaries. That is the case also for the 26.57°-twist grain boundary for which the quantity $\gamma_{WC/WC}-2\gamma_{Co/WC}$ is about 1.4 J/m^2. However, Eq. (10) is not satisfied for the $\Sigma=2$ boundaries as well as the W-W-I-*c* boundary which are strong enough to prevent binder penetration. As a consequence, the equilibrium morphology would not consist of isolated WC grains completely surrounded by a Co phase, but would instead contain some special WC/WC grain boundaries.

B. Application to liquid-phase sintering

During liquid-phase sintering of the cemented carbide, three different stages of densification can be distinguished, namely, rearrangement, solution reprecipitation, and coalescence, although the stages mix into each other. Each of these stages depends critically on the relations between the surface energies of the solid, liquid, and vapor phases as discussed by Gurland.[51]

At the initial stage of the densification, there is a mass transport of carbide particles through the liquid metal binder phase. The particles rearrange themselves to reduce the free energy of liquid-vapor interfaces, leading to denser packing and filling of the pores. A necessary condition for this to take place is that the liquid wets the particles. The success of the combination of Co and WC is to a large degree due to the extremely good wetting behavior of the metal on the carbide. Wetting experiments have shown that the wetting angle is close to zero,[49] allowing for a complete penetration of the metal phase into the voids between the carbide grains. The energetical requirement to avoid coalescence and assure mobility of the carbide grains is given by Eq. (10). It is highly unlikely that the good wetting properties of Co on WC necessary during this stage of sintering can be explained by the interfacial interactions underlying Fig. 8(a). The situation should be closer to the adhesion properties described by Fig. 8(b), where the Co/WC interface energy is minimized. The wetting condition is then fulfilled for WC grain boundaries with a high misorientation, which is the normal case for randomly oriented grains.

In the next stage of sintering, the densification is primarily due to a solution-reprecipitation process. The driving force is still a change of the free energy associated with the liquid-vapor interfaces and the conditions for the surface energy relationships are the same as in the first stage. The solubility of WC into the Co binder are increases with temperature and is quite high at normal liquid phase sintering temperature (1300–1500°C). The binder dissolved WC diffuse and reprecipitate elsewhere of the solute. This process is much more rapid at temperatures above solid-state sintering due to the activated viscous flow of the metal phase. The capillary pressure at the contact points of the solid grains leads to an enhanced activity of the solid phase resulting in a higher solubility in this area.[52] Carbide grains with an irregular shape can recrystallize and develop habit faces with low energy. If these low-energy habit faces come in contact, the grains can coalesce. The driving force for this process is the associated decrease of the solid-liquid interface free energy. It is most likely during this coalescence stage of sintering that the rigid WC skeleton is formed. This is in agreement with dilatometric infiltration experiments by Gurland[51] showing that a skeleton structure cannot be present at the early stages of liquid-phase sintering. However, experiments have shown that contiguity decreases with sintering time accompanied by considerable WC grain growth.[53] One explanation for the decrease in contiguity with time can be that Co penetrates the WC grain boundaries and breaks the WC agglomerates. At the same time, a limited contact of high coincidence boundaries associated with a low energy is developed. This is supported by the fact that a tendency for high coincidence boundaries has been found.[23] The energy requirement for the carbide coalescence is that the WC/WC grain-boundary energy is lower than twice the Co/WC interface energy. This condition is satisfied for the $\Sigma=2$ grain boundary. This particular grain boundary is probably formed in the recrystallization-coalescence stage of the sintering.

IX. SUMMARY

To optimize the properties of the cemented carbide, an understanding of the interface energy relationships involving the prismatic and basal planes is important. We have analyzed WC$\{10\bar{1}0\}$/WC$\{10\bar{1}0\}$ grain boundaries and Co(001)/WC$\{10\bar{1}0\}$ interfaces. An assessment of the properties of generic interfaces is obtained from three high-symmetry local interfacial configurations. We believe that this approach can be applied to a broad range of interface systems to get generic information from first principles at a low computational cost.

There are two types of WC$(10\bar{1}0)$ surfaces differing in the number of surface broken bonds. Type-I surfaces are more stable with a lower surface energy than the type-II surfaces. WC/WC and Co/WC interfaces involving either of these surfaces are generally strong, and the carbide-carbide grain boundaries and metal-carbide interfaces are comparable in strength. At the Co(001)/WC$(10\bar{1}0)$ interface, a very good wetting behavior of Co on WC is obtained if the Co atoms in the interface layer are allowed to attain the energetically most favorable positions with respect to the WC surface. The ability of the metal to locally adjust the atomic positions at the interface may be a prerequisite of good wetting for many metal-carbide systems.

There are also indications that the WC surface probably consists of a mixed composition of carbon and tungsten atoms. This statement is based on calculations using the WC(001) surface of β-WC. The WC(001) surface energy is lower than the WC$(10\bar{1}0)$ surface energy. Furthermore, the Co(001)/WC$(10\bar{1}0)$ work of separation is higher than the experimental value which is close to the corresponding value of the Co(001)/WC(001) interface.

According to the calculated energies, there clearly are carbide grain boundaries which in equilibrium will contain Co. This should be the case for grain boundaries formed by a random matching of WC$(10\bar{1}0)$ surfaces. However, no metal phase should reside in the singular $\Sigma=2$ grain boundary, which is consistent with microanalysis experiments.[25] It

should be noted that this does not exclude cobalt in submonolayer proportions in the $\Sigma=2$ boundaries.[54]

Moreover, the interface energy relationships in WC-Co during different stages of liquid-phase sintering are studied, resulting in a model for how these grain boundaries are formed. In this model, the $\Sigma=2$ grain boundaries are formed by coalescence of low-energy surfaces in the latter part of the sintering after the formation by a solution-reprecipitation process of low-energy crystallographic facets.

It can be concluded that the $\Sigma=2$ grain boundary which contains a very high number of coincidence sites is a particularly strong interface. No experimental evidence of Co has been found in this grain boundary. It is reasonable to believe that the hard WC skeleton at least partially consists of such interfaces.

ACKNOWLEDGMENTS

The idea of this work originates from discussions with U. Rolander, Sandvik Coromant AB, and H.-O Andrén, Chalmers. We are also thankful to S.V. Dudiy for very helpful discussions. This work was supported by the Swedish Foundation for Strategic Research (S.S.F.) and the Swedish Research Council (V.R.). Allocation of computer time at the UNICC facilities at Chalmers University of Technology is gratefully acknowledged.

[1] H.E. Exner, Int. Met. Rev. **24**, 149 (1979).
[2] M. Christensen, S.V. Dudiy, and G. Wahnström, Phys. Rev. B **65**, 045408 (2002).
[3] M. Christensen and G. Wahnström (unpublished).
[4] S. Hagège, G. Nouet, and P. Delavignette, Phys. Status Solidi A **61**, 97 (1980).
[5] T. Suzuki, K. Shibuki, T. Suzuki, and Y. Ikuhara, Philos. Mag. Lett. **71**, 289 (1995).
[6] P. Hohenberg and W. Kohn, Phys. Rev. **136**, B864 (1964).
[7] W. Kohn and L. Sham, Phys. Rev. **140**, A1133 (1965).
[8] R.O. Jones and O. Gunnarsson, Rev. Mod. Phys. **61**, 689 (1989).
[9] K. Reuter and M. Scheffler, Phys. Rev. B **65**, 035406 (2001).
[10] G.-X. Qian, R.M. Martin, and D.J. Chadi, Phys. Rev. B **38**, 7649 (1988).
[11] G. Kresse and J. Furthmüller, Phys. Rev. B **54**, 11 169 (1996).
[12] G. Kresse and J. Hafner, Phys. Rev. B **47**, 558 (1993).
[13] G. Kresse and J. Hafner, Phys. Rev. B **49**, 14 251 (1994).
[14] G. Kresse and J. Furthmüller, Comput. Mater. Sci. **6**, 15 (1996).
[15] J.P. Perdew, J.A. Chevary, S.H. Vosko, K.A. Jackson, M.R. Pederson, D.J. Singh, and C. Fiolhais, Phys. Rev. B **46**, 6671 (1992).
[16] M.C. Payne, M.P. Teter, D.C. Allan, T.A. Arias, and J.D. Joannopoulos, Rev. Mod. Phys. **64**, 1045 (1992).
[17] D. Vanderbilt, Phys. Rev. B **41**, 7892 (1990).
[18] G. Kresse and J. Hafner, J. Phys.: Condens. Matter **6**, 8245 (1994).
[19] H.J. Monkhorst and J.D. Pack, Phys. Rev. B **13**, 5188 (1976).
[20] P. Blöchl, O. Jepsen, and O.K. Andersen, Phys. Rev. B **49**, 16 223 (1994).
[21] F.D. Murnaghan, Proc. Natl. Acad. Sci. U.S.A. **30**, 244 (1944).
[22] A.V. Shatov, S.A. Firstov, and I.V. Shatova, Mater. Sci. Eng., A **242**, 7 (1998).
[23] J. Vicens, E. Laurent-Pinson, J.L. Chermant, and G. Nouet, J. Phys. Colloq. **49**, 271 (1988).
[24] J. Vicens, M. Benjdir, G. Nouet, A. Dubon, and J.Y. Laval, J. Mater. Sci. **29**, 987 (1994).
[25] J. Vicens, A. Dubon, J.Y. Laval, M. Benjir, and G. Nouet, J. Phys. Colloq. **51**, 347 (1990).
[26] D.L. Price and B.R. Cooper, Phys. Rev. B **39**, 4945 (1989).
[27] A.Y. Liu, R.M. Wentzcovitch, and M.L. Cohen, Phys. Rev. B **38**, 9483 (1988).
[28] S.V. Dudiy and B.I. Lundqvist, Phys. Rev. B **64**, 045403 (2001).
[29] E.G. Moroni, G. Kresse, J. Hafner, and J. Fürthmüller, Phys. Rev. B **56**, 15 629 (1997).
[30] L.F. Mattheiss and D.R. Hamann, Phys. Rev. B **30**, 1731 (1984).
[31] A.L. Ivanovskii, D.L. Novikov, and V.A. Gubanov, Phys. Status Solidi B **141**, 9 (1987).
[32] B. Roebuck and E.A. Almond, Int. Mater. Rev. **33**, 90 (1988).
[33] S.V. Dudiy, Surf. Sci. **497**, 171 (2002).
[34] D.J. Siegel, L.G. Hector, Jr., and J.B. Adams, Surf. Sci. **498**, 321 (2002).
[35] W. D. Jones, *Fundamental Principles of Powder Metallurgy* (Edward Arnold, LTD, London, 1960), p. 469.
[36] W. J. Huppmann and G. Peetzow, *Modern Developments in Powder Metallurgy*, edited by P. V. Taubenblatt and H. H. Hausner (Metal Powder Industries Federation, Princeton, NJ, 1977), Vol. 9, pp. 77–89.
[37] S. Kurth, J.P. Perdew, and P. Blaha, Int. J. Quantum Chem. **75**, 889 (1999).
[38] K. Carling, G. Wahnström, T.R. Mattsson, A.E. Mattson, N. Sandberg, and G. Grimvall, Phys. Rev. Lett. **85**, 3862 (2000).
[39] H. W. Hugosson, Ph.D. thesis, Uppsala University, Uppsala, 2001.
[40] K.L. Håkansson, H.I.P. Johansson, and L.I. Johansson, Phys. Rev. B **49**, 2035 (1994).
[41] J. Brillo, A. Hammoudeh, H. Kuhlenbeck, N. Panagiotides, S. Schwegmann, H. Over, and H.-J. Freund, J. Electron Spectrosc. Relat. Phenom. **96**, 53 (1998).
[42] A. P. Sutton and R. A. Balluffi, *Interfaces in Crystalline Materials* (Clarendon, Oxford, 1995).
[43] X. Jiang, J. Fassbender, and B. Hillbrands, Phys. Rev. B **49**, 13 815 (1994).
[44] R.M. Wentzcovitch and M.L. Cohen, Phys. Rev. B **37**, 5571 (1988).
[45] A.Y. Liu and D.J. Singh, Phys. Rev. B **47**, 8515 (1993).
[46] M. Aldén, H.L. Skriver, S. Mirbt, and B. Johansson, Surf. Sci. **315**, 157 (1994).
[47] R. Warren, Metallography **9**, 183 (1976).
[48] R. Warren, J. Mater. Sci. **15**, 2489 (1980).
[49] L. Ramqvist, Jernkontorets Ann. **153**, 159 (1969).
[50] R. Benedek, D.N. Seidman, and C. Woodward, J. Phys.: Condens. Matter **14**, 2877 (2002).
[51] J. Gurland, Jernkontorets Ann. **147**, 4 (1963).
[52] W.D. Kingery, J. Appl. Phys. **30**, 301 (1958).
[53] J. Gurland, Int. Mater. Rev. **33**, 151 (1988).
[54] A. Henjered, M. Hellsing, H.-O. Andrén, and H. Nordén, Mater. Sci. Technol. **2**, 847 (1986).